Individual Tree AGB Estimation of *Malania oleifera* Based on UAV-RGB Imagery and Mask R-CNN

Maojia Gong [1], Weili Kou [2,*], Ning Lu [2], Yue Chen [3], Yongke Sun [2], Hongyan Lai [1], Bangqian Chen [4], Juan Wang [5] and Chao Li [6]

[1] College of Forestry, Southwest Forestry University, Kunming 650224, China; gongmaojia@163.com (M.G.); lhy19931006@163.com (H.L.)
[2] College of Big Data and Intelligent Engineering, Southwest Forestry University, Kunming 650224, China; ninglu@swfu.edu.cn (N.L.); sunyongke@swfu.edu.cn (Y.S.)
[3] College of Mechanics and Transportation, Southwest Forestry University, Kunming 650224, China; chenyue960504@163.com
[4] Rubber Research Institute (RRI), Chinese Academy of Tropical Agricultural Sciences (CATAS), Hainan Danzhou Agro-Ecosystem National Observation and Research Station, Haikou 571101, China; chbq40@163.com
[5] Eco-Development Academy, Southwest Forestry University, Kunming 650224, China; schima@163.com
[6] Cigarette Product Quality Test Center, Technology Center of China Tobacco Yunnan Industrial Co., Ltd., Kunming 650023, China; super88man66@126.com
* Correspondence: kwl@swfu.edu.cn

Abstract: Forest aboveground biomass (AGB) is an important research topic in the field of forestry, with implications for carbon cycles and carbon sinks. *Malania oleifera* Chun et S. K. Lee (*M. oleifera*) is a valuable plant species that is listed on the National Second-Class Protected Plant checklist and has received global attention for its conservation and resource utilization. To obtain accurate AGB of individual *M. oleifera* trees in a fast, low-finance-cost and low-labor-cost way, this study first attempted to estimate individual *M. oleifera* tree AGB by combining the centimeter-level resolution RGB imagery derived from unmanned aerial vehicles (UAVs) and the deep learning model of Mask R-CNN. Firstly, canopy area (CA) was obtained from the 3.5 cm high-resolution UAV-RGB imagery using the Mask R-CNN; secondly, to establish an allometric growth model between the diameter at breast height (DBH) and CA, the correlation analysis of both was conducted; thirdly, the AGB estimation method of individual *M. oleifera* trees was presented based on an empirical equation. The study showed that: (1) The deep learning model of Mask R-CNN achieved an average segmentation accuracy of 90% in the mixed forests to the extraction of the canopy of *M. oleifera* trees from UAV-RGB imagery. (2) The correlation between the extracted CA and field-measured DBH reached an R^2 of 0.755 (n = 96). (3) The *t*-test method was used to verify the predicted and observed values of the CA-DBH model presented in this study, and the difference in deviation was not significant ($p > 0.05$). (4) AGB of individual *M. oleifera* was estimated for the first time. This study provides a reference method for the estimation of individual tree AGB of *M. oleifera* based on centimeter-level resolution UAV-RGB images and the Mask R-CNN deep learning.

Keywords: *Malania oleifera*; aboveground biomass; UAV; Mask R-CNN; allometric growth model

1. Introduction

Malania oleifera Chun & S. K. Lee (*M. oleifera*) is a rare, high-value, and protected species of evergreen broad-leaved trees found in arid regions. It belongs to the genus *Malania* within the Olacaceae family and is highly valued for its fruits, leaves, and trunk [1]. The kernels of *M. oleifera* contain over 60% oil and can be used to extract edible and aromatic oils [2]. Its fruit oil is also rich in neuronic acid, an important material for treating neurological diseases and promoting brain growth and nerve regulation [2]. *M.*

oleifera is an important source of neuronic acid extraction and is a sustainable alternative to animal sources. Although marine animals also contain neuronic acid, the amount that can be extracted is limited, and the extraction of neuronic acid from marine animals has been explicitly banned [3]. Therefore, *M. oleifera* is an important source of neuronic acid extraction, instead of animal sources, as a new energy source for neuronic acid extraction and is sustainable. However, the current resources of the *M. oleifera* species are very limited; it is only found growing in Funing and Guangnan counties in eastern Wenshan Zhuang and Miao Autonomous Prefecture (Wenshan), Yunnan Province, and in the karst landscape areas of western Guangxi Zhuang Autonomous Region (Guangxi) in China [4,5], and is scattered in complex natural mixed forests. Therefore, it is urgent to investigate and protect *M. oleifera* resources, expand its planting area, and enhance the management and utilization of native *M. oleifera* resources. Biomass estimation is critical for monitoring plant growth and yield; however, aboveground biomass (AGB) estimation for *M. oleifera* has not been reported in the existing literature. Previous studies on *M. oleifera* have focused on plant cultivation, pests, diseases, oil extraction [3,6,7], extraction and isolation of volatile oil [7], and genome analysis [2,4], while its AGB estimation has not been reported yet.

AGB is a key parameter in characterizing life activities and is the most basic quantitative characteristic of forest ecosystems. It not only indicates the traits of plant growth, but also is of great significance for plant growth monitoring, yield estimation [8,9], industrialization development, and protection of germplasm resources. Additionally, it is also an important indicator to evaluate ecosystem health and carbon storage [10–12]. Trees are the mainstay of forest ecosystems, and individual tree biomass accounts for the majority of the biomass in ecosystems. Accurate estimation of individual tree biomass is highly essential for the quantification of forest biomass, carbon stocks, carbon channels, forest management, and climate changes. To accurately estimate forest AGB in complex forest stands, a reliable individual tree AGB model should first be constructed. Although the AGB estimation method based on traditional field investigations has the advantage of fine estimation accuracy at small scales, it is time-consuming and inefficient, physically impairs the trees, and is unsuitable for large areas [9,13]. In recent years, satellite remote sensing technology has been used to overcome the limitations of traditional estimation methods and has become an efficient way to evaluate forest AGB. Using satellite remote sensing technology to obtain forest parameters can reduce the damage to forests and save the output of the labor force and financial resources, and thereby achieve multi-scale, multi-temporal remote sensing [14–16]. Among these approaches, optical (such as Landsat, Sentinel-2, GF-1, GF-2) and synthetic aperture radar (such as Sentinel-1, GF-3) data are commonly used [14,17–21] to estimate forest AGB and can greatly improve the overall efficiency [15,18–23] compared to traditional methods. However, satellite remote sensing images are susceptible to cloud contamination and low spatial and temporal resolution, which makes it difficult to guarantee the quality of the acquired satellite images [23–25]. Although some research makes up for this shortcoming by using airborne methods to obtain satellite remote sensing images to improve their quality [26–28], because of their need for a high-cost and cumbersome process, they are not suitable for widespread applications.

With the rapid development of unmanned aerial vehicle (UAV) technology, UAVs have become a new remote sensing data acquisition platform. Different types of sensors mounted on UAVs can obtain a variety of high-resolution remote sensing images. More accurate forest parameters can be extracted from UAV high-resolution imagery than from satellites and can satisfy the requirements of mixed forest AGB estimation [29,30]. Remote sensing images derived from UAV-based RGB, multi-spectral, hyperspectral, light detection and ranging (LiDAR) sensors are extensively used to estimate the AGB of crops, trees, and grasslands, as well as predict their yield and monitor their growth [8,29–33]. Among these sensors, although other sensors perform better than the RGB sensor in AGB estimation [9,34–36], their application is seriously limited in practice due to their high costs and complex operations. RGB cameras have great potential in forest resources monitoring and AGB estimation, with the advantages of simple operations, low costs, and high spatial

resolution [24]. The parameters of texture, spectral information, structural indices, etc. have been extracted from UAV-RGB images and already used to successfully estimate the AGB of desert shrubs [29], corn [37], and rubber plantations [24].

There has been rapid development in the field of machine learning in recent years, which has been widely used in the estimation of biomass, identification of tree species, and classification of trees. As an important subset of machine learning, the deep learning method is represented by the Convolutional Neural Network (CNN). The CNN extracts deep features of images by training a large amount of data and has achieved excellent results in image recognition, classification, segmentation, and remote sensing [38–41]. It also shows great potential in individual tree detection, classification, and tree canopy segmentation in the study of remote sensing data [39,41]. High-precision tree species can be recognized using deep learning algorithms combined with hyperspectral data or UAV-RGB remote sensing images [40,42]. In recent years, the deep learning algorithms of AlexNet, ResNet, and Mask R-CNN were extensively used to extract tree height [43], segment individual trees [44], and estimate forages AGB [45] in combination with UAV-RGB remote sensing images. Furthermore, the deep learning algorithm has tremendous potential in extracting mixed forest parameters, tree species identification, and estimating AGB. It can also greatly improve the analysis accuracy and reduce the output of material and financial resources [39–41]. In particular, Mask R-CNN can achieve high recognition accuracy in highly depressed forest fractions [44]. Thus, Mask R-CNN deep learning algorithms provide a new way to identify and extract tree canopies of *M. oleifera* for AGB estimation and yield prediction.

Canopy Area (CA) can be aerially and visually measured on remote sensing images, but the diameter at breast height (DBH) needs to be investigated in the field, which is time-consuming and laborious [34,46]. Fortunately, there is a high correlation between CA and DBH [42,43], so DBH can be estimated by CA measured from high-resolution remote sensing based on the allometric growth model. As a scattered tree species, *M. oleifera* is sporadically distributed in complex mixed natural forest stands, and traditional methods to identify their canopies are very difficult to apply. However, it is highly feasible to identify and extract the canopy of this species using UAV high-resolution remote sensing images combined with deep learning algorithms.

Therefore, this study aimed to detect *M. oleifera* canopies in complex forests using the Mask R-CNN model based on high-resolution remote sensing images acquired from RGB sensors mounted on UAVs. Exploring the effectiveness of Mask R-CNN models for *M. oleifera* canopy recognition and the individual CA of *M. oleifera* was conducted using the ArcGIS10.7 software. Technical support was provided for the survey of *M. oleifera* resources and the acquisition of forest parameters. Secondly, a CA-DBH anisotropic growth model was constructed using field measurements of DBH and CA to analyze the anisotropic growth relationship. Finally, the empirical equation of the AGB of *Cinnamomum camphora* based on the DBH parameter was used to estimate the AGB of individual *M. oleifera*. As the first attempt to estimate the AGB of *M. oleifera*, this study can provide a methodological reference for estimating the AGB of *M. oleifera*, and then provide technical support for *M. oleifera* resource monitoring and yield prediction.

2. Materials and Methods

2.1. Study Area

The study area is situated in Funing county, Wenshan, Yunnan Province, China, within the coordinates of 105°13′–106°12′ E and 23°11′–24°09′ N. It is bordered by Guangxi in the east and north, which is adjacent to Ha Giang Province Vietnam, Guangnan, and Malipo counties in the west of Wenshan. The sampling was mainly conducted in Mudu village, Banlun township, Funing county, which is located at an altitude of 1440 m and has an average annual temperature of 19.8 °C and annual precipitation of 1378.8 mm. This area is more densely populated with the natural distribution of *M. oleifera* (Figure 1).
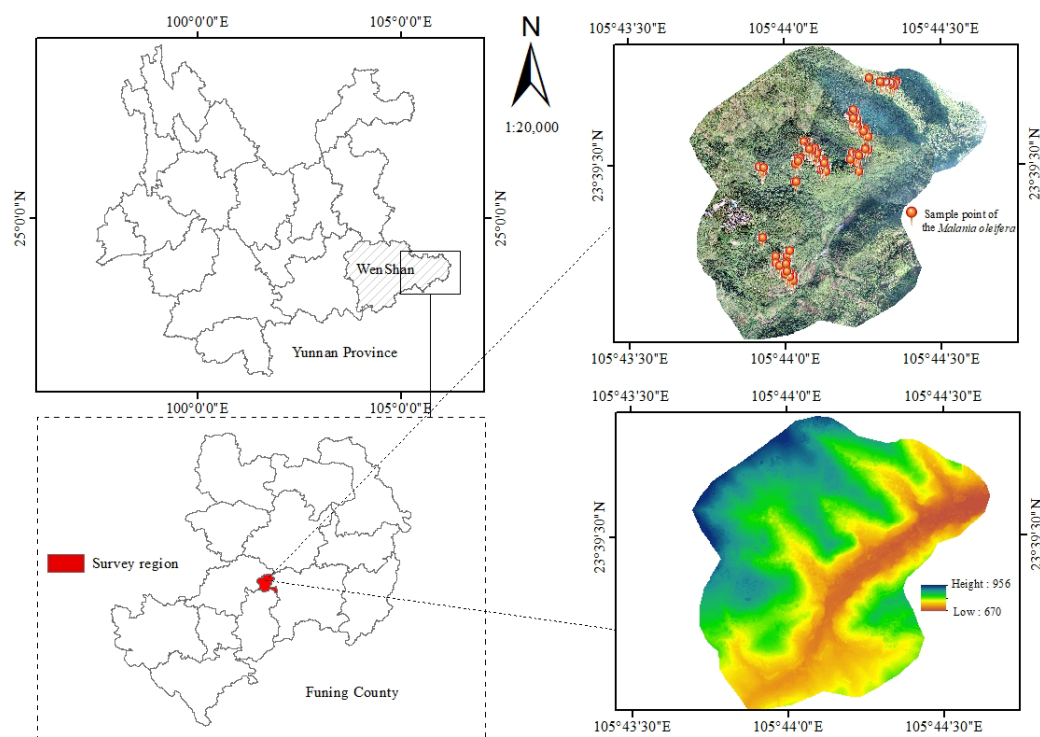
Figure 1. The location of the study area.

2.2. Field Surveys of M. oleifera

In order to identify the canopies of *M. oleifera* in high-resolution UAV-RGB images, the study relied on a combination of field surveys and image analysis. Field surveys were conducted from 17 to 19 January, on 17 April, and from 23 to 24 April in 2021. Because *M. oleifera* grows in rocky mountain environments, the field survey was conducted under the leadership of local rangers. The *M. oleifera* with DBH ≥ 5 cm was measured by a diameter ruler at a height of the trees of 1.3 m. The tree height of *M. oleifera* was acquired by a direct reading altimeter. A real-time kinematic instrument called ZHD V200 (RTK, Guangzhou Hi-Target Navigation Tech Co., Ltd., Guangzhou, China) was used to determine the geographic location of the *M. oleifera*. The DBH, tree height, and location of a total of 217 *M. oleifera* trees were collected for subsequent processing and analysis.

2.3. UAV-RGB Imagery Acquisition and Preprocessing

This study employed a DJI Phantom 4 RTK multi-rotor drone with an integrated new RTK module and a new Time Sync system with a 1″ CMOS sensor to acquire true color (RGB) images in JPEG format with a resolution of 5472 × 3648 pixels (Table 1). The flight campaign was conducted at between 10:00 a.m and 3:00 p.m in the local time on 17 April 2021 during the flowering stage of *M. oleifera*. Given the large elevation difference of the study area, we utilized the terrain awareness flight mode of the DJI Phantom 4 RTK system to obtain the same resolution RGB images. The 30 m digital elevation model (DEM) of the study area was downloaded from the Earthdata website (https://data.nasa.gov/ accessed on 20 March 2021), and was processed into terrain data supported by the DJI flight control system. To cover the entire investigation area and ensure flight safety, the study area was divided into multiple subareas based on terrain changes. Therefore, multiple flights were carried out to acquire high-resolution RGB imagery of *M. oleifera* at the same flight height of 100 m. To generate an orthophoto to cover the entire study site, the forward and side overlaps were set to 80% and 70%, respectively.

Table 1. The UAV system parameters.

Parameters	Numerical and Descriptive	Parameters	Numerical and Descriptive
UAV models	DJI Phantom 4 RTK	Range of obstacle perception/m	0.2–7
Flight height	100 m	Image sensors	1″ CMOS; 20 million effective pixels
Forward overlapping	80%	Photograph resolution/pixels	5472 × 3648 (3:2) 4864 × 3648 (4:3)
Side overlapping	70%	Spatial resolution/cm	2.74

In this study, based on UAV-RGB, 2547 images of the *M. oleifera* research area were collected, excluding distorted ones. Agisoft metashape (Agisoft LLC, St. Petersburg, Russia) software was used to splice the images obtained by the UAV to obtain digital orthophoto map (DOM) and digital surface model (DSM) data. The stitching process is shown in Figure 2.
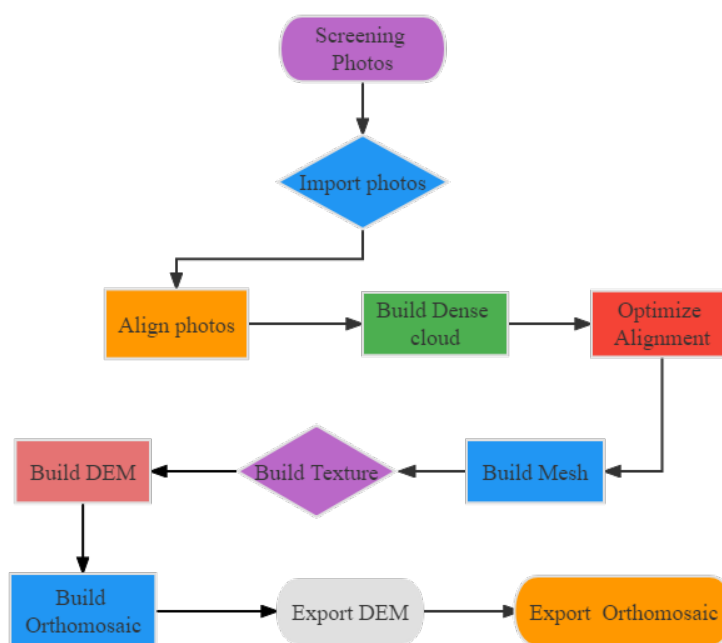
**Figure 2.** UAV image stitching process.

2.4. The Canopy Detection of M. oleifera Trees Using Mask R-CNN

The Mask R-CNN network segmentation algorithm was used to extract tree canopies, as it has been shown to perform better in semantic segmentation compared to traditional algorithms [47]. The algorithm is improved based on Faster R-CNN, incorporating ideas from Fully Convolutional Networks (FCNs) and Feature Pyramid Networks (FPNs) with a Mask branch. The Mask R-CNN has two processing stages; the first stage is responsible for extracting image features, and the second stage predicts the location and category of each region of interest, as well as masking for the target object [47,48]. The architecture of Mask R-CNN is shown in Figure 3. In this study, the Mask R-CNN model construction and application of the implementation were based on the detectron2 (https://github.com/facebookresearch/detectron2 accessed on 15 November 2021) platform. Firstly, the *M. oleifera* trees in images acquired by the UAV-RGB camera were manually annotated by the "Labelme" (https://github.com/wkentaro/labelme accessed on 28 November 2021) image annotation tool to generate a file in JSON format. Then, all images were split into training images (1016) and testing images (254). The Mask R-CNN model was used to perform canopy segmentation analysis with an image size of 800 × 800 pixels and 120,000 iterations.
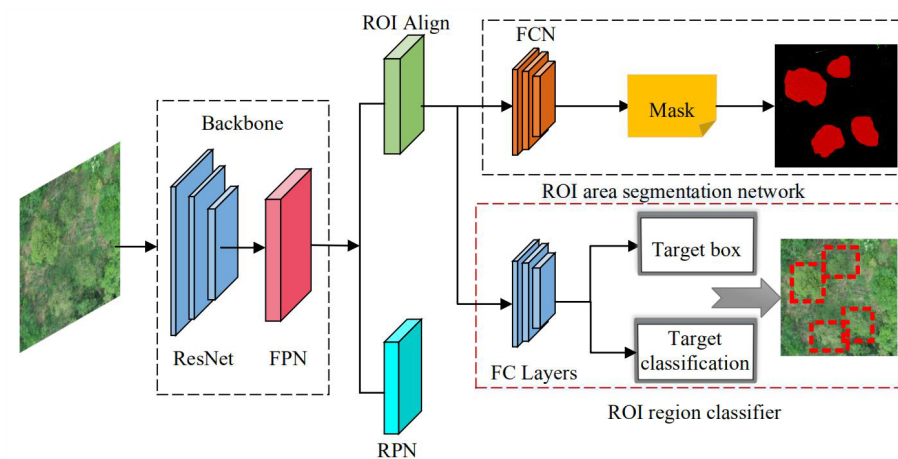
Figure 3. Mask R-CNN architecture diagram.

The Mask R-CNN was trained using a training data set. The loss value change curve during training shows that iteration stabilization occurred in the range between 10,000 and 120,000 and finally converged to about 0.03 (Figure 4).
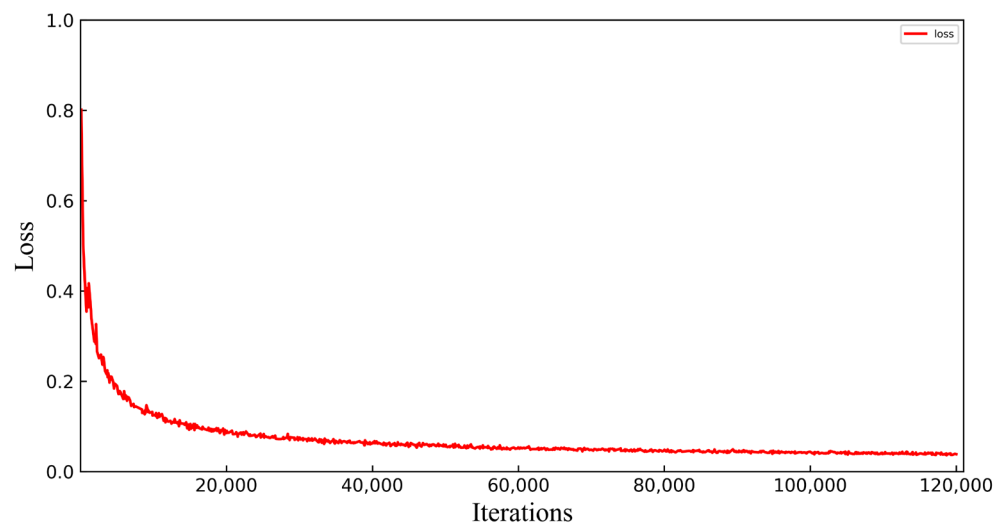
Figure 4. Change in loss values for different iterations.

An important application of the Mask R-CNN model is tree canopy detection and delineation. During the computation, the model provides an overlapping threshold to average the detection results to avoid bias. The overlapping threshold here refers to the intersection over union (*IoU*, Equation (1)) between an individual candidate box and the actual annotated box. In object detection and segmentation tasks, the *IoU* is a metric used to evaluate the accuracy of predicted bounding boxes or segmentation masks.

$$IoU = \frac{S_{A \cap B}}{S_{A \cup B}} \tag{1}$$

where A represents the real object area and B represents the predicted bounding box or segmentation mask. The *IoU* value is calculated as the ratio between the intersection area of A and B and the union area of A and B. The *IoU* value ranges from 0 to 1, where a higher value indicates a better prediction accuracy of the bounding box or segmentation mask. This segmentation result is True Positive (*TP*) when $IoU \geq 0.5$, False Positive (*FP*) when $IoU < 0.5$, and False Negative (*FN*) when the individual wood canopy is incorrectly detected as background.

This research evaluated the accuracy of the Mask R-CNN model for *M. oleifera* individual tree canopy segmentation using recall (*R*, Equation (2)), precision (*P*, Equation (3)), and *F*1-score (Equation (4)). The purpose of this evaluation was to determine the performance of the model and provide insights into its strengths and weaknesses. By evaluating the model using these metrics, we can determine its accuracy in identifying *M. oleifera* individual tree canopy segments. This can help improve the model and its performance in future applications.

$$R = \frac{TP}{TP + FN} \tag{2}$$

$$P = \frac{TP}{TP + FP} \tag{3}$$

$$F1\text{-}score = 2 \times \frac{P \times R}{P + R} \tag{4}$$

where *TP* is True Positive, *FP* is False Positive, *FN* is False Negative, *R* represents the recall, and *P* represents the precision.

2.4.1. *M. oleifera* Tree Canopy Recognition Results

According to the data in Table 2, the Mask R-CNN model can identify most of the individual tree canopies of *M. oleifera* against a complex stand background. However, due to canopy aggregation, connection, and even overlap in the growth area of *M. oleifera*, there are still under-segmentation or difficult segmentation problems.

Table 2. Evaluation of individual tree canopy segmentation results.

Segmentation Results			Segmentation Accuracy Evaluation Results		
TP	**FN**	**FP**	**Recall**	**Precision**	**F1-Score**
141	30	16	83%	90%	86%

Individual tree canopy segmentation tests were carried out on the test set by the trained Mask R-CNN model. The results of individual tree canopy splitting of *M. oleifera* were obtained (Figure 5) and the segmentation accuracy was 90%.
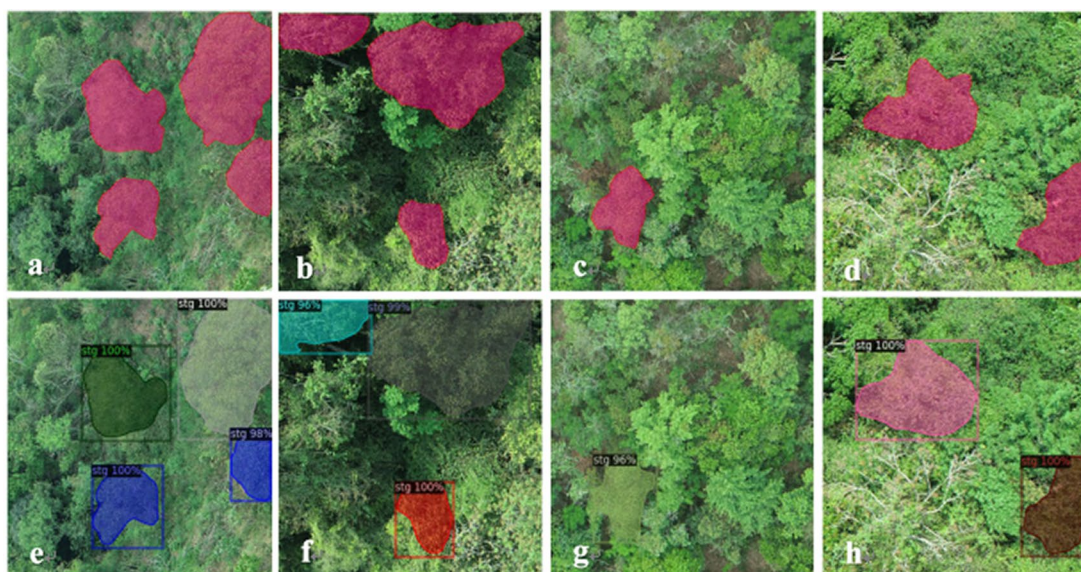
Figure 5. The canopy segmentation results in comparison of manual-visual interpretation and the Mask R-CNN: (**a**–**d**) are manual-visual interpretation results; (**e**–**h**) are the Mask R-CNN results.

2.4.2. CA Extraction

Real-time kinematic (RTK) differential techniques can eliminate ionospheric, tropospheric, and other errors, and these techniques greatly improve the accuracy of the measurement. In this study, the geographic coordinate points of *M. oleifera* were obtained through RTK, and the images were processed by the overlay analysis tool in ArcGIS10.7 software (https://www.arcgis.com/ accessed on 5 November 2020). The outline range of the *M. oleifera* during the field survey was used to merge the over-segmented canopies and to adjust the parts of the *M. oleifera* that were outside the canopy (Figure 6).

(a) (b)

Figure 6. The Mask R-CNN model for extracting *M. oleifera* canopies compared with the original image: (**a**) the original tree canopy image, (**b**) the extracted tree CA.

2.5. AGB Estimation of M. oleifera

2.5.1. Establishment and Effectiveness of Allometric Growth Equation

The establishment of the allometric growth equation is a common non-destructive method of estimating AGB, and its basic mathematical model is a power function. Figure 7 shows the relationship between DBH and CA. The linear model, power function model, and polynomial model were chosen to fit the data. The power function returned the largest R^2 and was chosen as the optimal equation to fit the data, and DBH was selected as the independent variable. The allometric equation for CA-DBH was built as Equation (5):

$$D = aC^b \tag{5}$$

where D is the diameter at breast height of *M. oleifera* measured by the field survey, C is the canopy area of individual *M. oleifera* obtained from UAV-RGB remote sensing images, and a and b are the relevant parameters obtained by regressing the obtained CA and DBH.

To build a reliable CA-DBH model, the DBH data collected in the field survey corresponding to the 120 CAs extracted based on Mask R-CNN were divided into 80% (96) for model calibration and 20% (24) for model validation using a k-fold cross validation approach (in this case, 5-fold) [49,50]. The coefficient of determination (R^2, Equation (6)) and the significance (P) were used to evaluate the fitting results. The predicted and observed values were subjected to a *t*-test. The reliability of the model was verified and evaluated using the mean absolute error (*MAE*, Equation (7)), the root mean square error (*RMSE*, Equation (8)), the relative root mean square error (*rRMSE*, Equation (9)), and the *Bias* (Equation (10)).

$$R^2 = 1 - \frac{\sum_{i=1}^{n}(y_i - \hat{y}_i)^2}{\sum_{i=1}^{n}(y_i - \overline{y})^2} \tag{6}$$

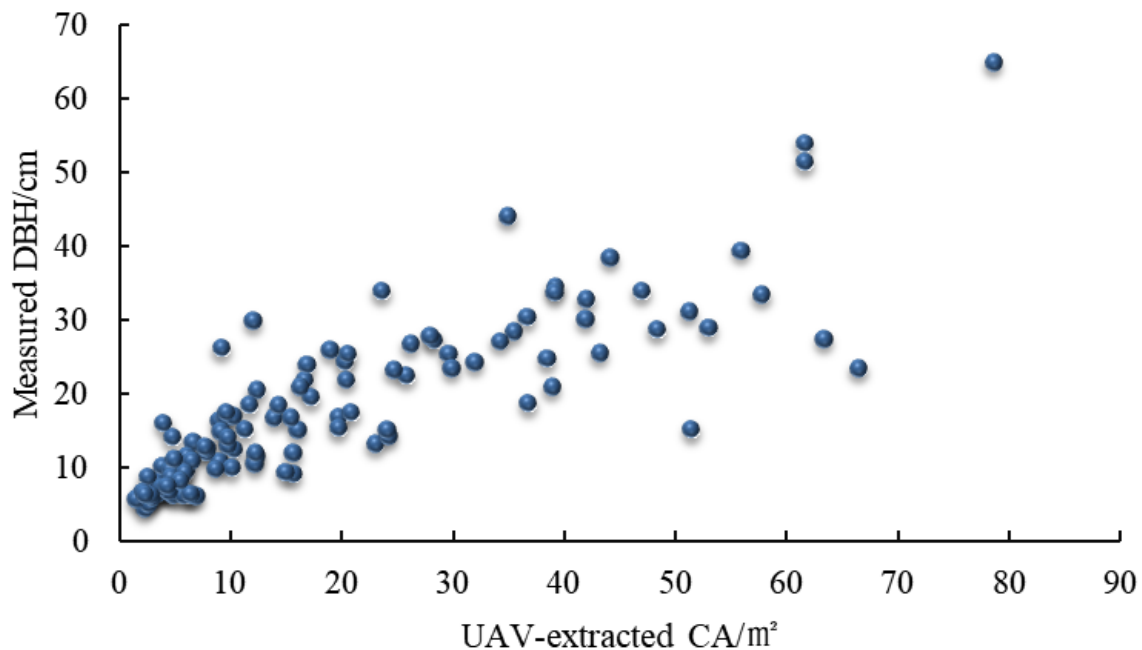$$MAE = \frac{\left(\sum_{i=1}^{n}\left|y_i - \hat{y}_i\right|\right)}{n} \tag{7}$$

$$RMSE = \sqrt{\frac{\left(\sum_{i=1}^{n}(y_i - \hat{y}_i)^2\right)}{n}} \tag{8}$$

$$rRMSE = \sqrt{\frac{(\sum_{i=1}^{n}(y_i - \hat{y}_i)^2)/n}{\bar{y}_i}} \tag{9}$$

$$Bias = \frac{\sum(\hat{y}_i - y_i)}{n} \tag{10}$$

where y_i represents the measured value, $\hat{y}_i$ represents the predicted value, $\bar{y}_i$ represents the average value, and n represents the sample size.

Figure 7. The scatter diagram of CA and DBH.

2.5.2. Selection of Empirical Equation

M. oleifera is an ancient and high-value species, classified as a National Second-Class Protected Plant, and is rich in oil and nervonic acid. However, its AGB cannot be estimated by the traditional parsed wood method. Taxonomically, *M. oleifera* was previously classified under Lauraceae, and it has the odor of Lauraceae; furthermore, the species of the Camphor family are evergreen broad-leaved woody oil plants [51]. Their morphological characteristics and growth environment are also relatively similar (Table 3). *M. oleifera* and *Cinnamomum camphora* have similarities in morphological characteristics, with both having distinctive features such as dried flowers, petals, stamens, and styles. In addition, the leaves of both also have some similarities, both presenting a deformed ovate or obovate shape. In terms of ecological and geographic distribution patterns, both prefer to grow in areas with abundant rainfall, a warm climate, and fertile soil. *M. oleifera* is mainly distributed in southern provinces such as Yunnan and Guangxi, while *Cinnamomum camphora* is widely distributed in southern China and Southeast Asia [7,51]. In summary, the *M. oleifera* and *Cinnamomum camphora* have similarities in morphological characteristics, ecological environment, geographical distribution, and growth habits. Therefore, the AGB of *M. oleifera* was estimated with the empirical AGB equation of *Cinnamomum camphora* [52]

$$W = 0.147 \times D^{2.191} \tag{11}$$

where *W* is the whole AGB of a tree.

Table 3. The comparison of *M. oleifera* and *Cinnamomum camphora*.

Species of Trees	Morphological Characteristics	Growth Habits
M. oleifera	Evergreen trees with slightly longitudinally fissured bark, having alternate leaves with semi-cylindrical petioles. They flower from April to September and fruit from May to October.	Subtropical evergreen broad-leaved species, M. oleifera is commonly found growing in mountainous areas at altitudes ranging from about 300–1200 m. It prefers moist, fertile soils and is often found on limestone hills, but can also grow on acidic soils in sandstone and shale areas [51].
Cinnamomum camphora	Evergreen trees; bark with irregular longitudinal fissures; leaves alternate, ovate-elliptic; flowering Apr-May, fruit period August-November.	Subtropical evergreen broad-leaved species adapted to altitudes below 1800 m, and is light-loving, slightly shade-tolerant, and prefers a warm and humid climate. It is suitable for deep fertile acidic or neutral sandy loam soils [53,54].

3. Results and Analysis

3.1. CA Extraction of M. oleifera Trees Based on UAV-RGB Images

The Mask R-CNN algorithm was utilized to extract the contours of *M. oleifera* canopies for a total of 120 plants, achieving an average recognition accuracy of 90% and recall of 83%. The resulting tree canopy profiles were imported into ArcGIS10.7 software (https://www.arcgis.com/ accessed on 5 November 2020), and the CA was calculated. The DBH varied from 5.00 to 65.00 cm, with a mean value of 17.66 cm, while the CA ranged from 1.500 to 78.58 m^2, with a mean value of 18.62 m^2 (Table 4).

Table 4. The CA extraction results of *M. oleifera* based on UAV-RGB images.

Sample	Value
n	120
DBH range/cm	5.00–65.00
Average DBH/cm	17.66
CA range/m^2	1.50–78.58
Average CA/m^2	18.62

3.2. The CA-DBH Model of Individual M. oleifera Tree

The regression analysis results of the power function, linear, and polynomial models indicated a strong correlation between CA and DBH, with an R^2 value above 0.8 for all models (Table 5). Among the three models, the power function model was identified as the optimal one for establishing the anisotropic growth model between CA and DBH (Equation (12)).

$$D = 3.825 \times C^{0.546} \tag{12}$$

where *D* is the DBH of the *M. oleifera* and *C* is the area of the individual *M. oleifera* canopy measured by UAV-RGB remote sensing images.

Table 5. The fitting results of different models.

No.	Models	R^2
1	Power function	0.755
2	Polynomial	0.739
3	Linear function	0.732

A *t*-test was performed on the predicted and observed values of the CA-DBH model for 20% (24) of the validation data set (Table 6). The results showed that the bias of the DBH predicted by the CA-DBH model and measured DBH was 1.03 cm. The deviation between the predicted and observed values of the model was not significant ($p > 0.05$).

Table 6. The *t*-test results of the measured and predicted values of DBH of *M. oleifera* in the sampled data.

No.	Index	Value
1	Mean field measured/cm	17.66
2	The standard deviation of field measured/cm	10.91
4	Mean UAV—predicted/cm	16.98
5	The standard deviation of predicted values	9.11
	The coefficient of determination R^2	0.71
6	Root means square error (RMSE)/cm	5.38
7	Mean absolute error (MAE)/cm	3.79
8	Relative root means square error (rRMSE)/cm	1.27
9	Bias/cm	1.03

3.3. The AGB Estimation of Individual M. oleifera Trees

The empirical equation for the AGB of *Cinnamomum camphora* (Equation (11)) combines the fitted CA-DBH model (Equation (12)) to estimate the AGB of individual *M. oleifera* trees. The measured DBH was used as validation data to estimate the biomass. The results indicated that a good estimation accuracy (R^2 = 0.69, MAE = 23.04 kg, RMSE = 34.03 kg, rRMSE = 3.56 kg, Bias = 6.94 kg) was achieved for the AGB of individual *M. oleifera* trees.

4. Discussion

4.1. The Advantages of UAV-RGB Imagery in Estimating CA in Natural Mixed Forests

Traditional field investigations for estimating forest AGB can be subjective and lead to deviations in estimates due to different investigator experiences. In recent years, the use of UAV remote sensing technology has rapidly risen in agriculture, forestry, and other fields. As a high-value tree species, *M. oleifera* is sporadically distributed in natural mixed forests and is difficult to investigate in the field. Consequently, UAV remote sensing technology is an efficient way to investigate *M. oleifera* resources. Although many scholars have used satellite remote sensing images to estimate forest AGB over the past decades [18,22], it is difficult to estimate the AGB of natural mixed forests using satellite images with relatively coarse resolution. In contrast, UAV-RGB sensors have centimeter-level resolutions and can provide different image resolutions by adjusting the flight height. The CA can be accurately measured, through UAV-RGB centimeter-level imagery, by investigators indoors (Figure 8). This study set the flight altitude to 100 m, and the resolution of the UAV-RGB images was about 3.5 cm. The flight mode of imitating landforms is an efficient solution to the problem of terrain ups and downs. It provides the best image data source for quick and accurate extraction of *M. oleifera* canopy information. Additionally, the accuracy of the canopy extracted by the deep learning algorithm was further improved, providing data sources and technical references for resource management and the development of the utilization of *M. oleifera*.

4.2. The Performance of Mask R-CNN for Obtaining CA of M. oleifera Trees in Natural Mixed Forests

The Mask R-CNN is a network for object detection and segmentation based on Faster R-CNN and is extensively used in the technology of image detection, recognition, and segmentation [47]. Yang Changhui et al. [55] used Mask R-CNN to identify the branches of citrus trees, and the average recognition accuracy reached 98.15%. In this study, the CA-DBH allometric growth model was established based on CA and DBH; thus, accurate extraction of the canopy contour was very crucial for the regression model. Based on UAV-RGB imagery with a spatial resolution of about 3.5 cm, the Mask R-CNN model was used to detect and extract the canopy of *M. oleifera*. Since *M. oleifera* is sporadically distributed in natural mixed stands, the stand environment is more complex than artificially planted citrus orchards. The segmentation accuracy of the *M. oleifera* canopy in this study was 90% and the average recall was 83%. This shows that the Mask R-CNN model used

in this study can recognize the canopy of trees in natural mixed forests and improve CA measurement efficiency.

Figure 8. The comparison of satellite remote sensing and centimeter-level UAV-RGB imagery: (**A**) is a satellite remote sensing image with a spatial resolution of 0.6 m; (**B**) is the UAV-RGB imagery with a resolution of 3.5 cm.

It is a meaningful achievement to quickly and efficiently identify a tree species and extract its canopy information in a complex forest stand. The Mask R-CNN model is capable of automatically retrieving accurate CA from UAV-RGB centimeter-level remote sensing images. Meanwhile, the accurate RTK coordinates of the *M. oleifera* collected in the field survey are beneficial to delineate the final *M. oleifera* CA. The canopy boundary of the *M. oleifera* tree extracted based on the Mask R-CNN model was trimmed with the canopy contours outlined in field investigations, which improved the AGB estimation of individual *M. oleifera* trees.

4.3. The Optimal CA-DBH Allometric Growth Model of M. oleifera

This study separately used the linear, polynomial, and power function models to fit the CAs measured from UAV-RGB images with DBHs investigated in the field of *M. oleifera*, and their R^2 of all fitting results was above 0.8. This illustrates that there is a high correlation between them. The R^2 of the power function model is the highest among the three models and was selected to construct the CA-DBH allometric growth model in this study; other studies had similar findings [56]. It was further demonstrated that the power function model was more effective for modeling the heterogeneous growth rate of CA and DBH, and the biomass estimation using this method was reliable. In addition, the high correlation between CA and DBH of tall tree species such as fir and *M. oleifera* indicates that the use of CA to estimate the biomass of individual plants of *M. oleifera* is feasible.

4.4. AGB Estimation of M. oleifera

Due to *M. oleifera* being a National Second-Class Protected Plant, it was not possible in this study to cut the trees to construct an AGB model by traditional methods. Hence, the AGB model of *Cinnamomum camphora* was employed to estimate individual AGB values of the *M. oleifera* tree due to the similarity of the two species. Both of them are very similar in appearance and growth habits, belong to subtropical evergreen tree species, are photophilous plants, mainly grow in fertile soil areas below 1800 m altitude, and are characterized as woody oil plants with high oil content. Moreover, *M. oleifera* and *Cinnamomum camphora* were both initially classified as Lauraceae. This is a common approach for the study of rare species; for example, since *Aquilaria sinensis* is a rare medicinal plant and a national secondary protected species, its volume is calculated using the binary volume calculation formula of *Schima Crenata* [57]. Therefore, it was feasible in this study to estimate the AGB of the *M. oleifera* tree with the help of empirical equations used to estimate the biomass of *Cinnamomum camphora*.

This study is the first attempt to estimate the AGB of individual *M. oleifera* trees, which fills a gap in the study of the biomass of a special species. Although some studies found that the AGB is highly correlated with tree height, DBH, crown width, and wood density, more variables may increase the burden of data acquisition and processing [58]. Therefore, this study only used one parameter (DBH) to establish the AGB estimation model of individual *M. oleifera* trees. This idea is consistent with the previous study by Tang et al. (2009), which reported that the allometric growth model based on DBH achieved a high R^2 of 0.99 for the AGB of an individual rubber tree.

In addition, since *M. oleifera* is a key protected species and its measured AGB cannot be retrieved using a destructive sampling method, in this study, the existing empirical model of *Cinnamomum camphora* was used to obtain the measured AGB of *M. oleifera*. The two species have more similarities in terms of their morphological characteristics, ecological environment, geographical distribution, and growth habits. Nonetheless, we also tried to estimate the biomass of *M. oleifera* using the AGB estimation equation of *Pinus yunnanensis* (Franch) [59] and *Quercus* spp. [60], which are common tree species in Yunnan Province. The results showed consistent trends in estimating the AGB of *M. oleifera* using biomass estimation models of *Pinus yunnanensis*, *Quercus* spp., and *Cinnamomum camphora* (Figure 9). The results obtained using the *Cinnamomum camphora* biomass estimation equation were more similar to those obtained using the biomass estimation equation of *Pinus yunnanensis*, the most common tree species in Yunnan Province [61], further indicating that *Cinnamomum camphora* is the most suitable tree species for estimating AGB of *M. oleifera*. Of course, using the AGB estimation model of *Cinnamomum camphora* to estimate the AGB of *M. oleifera* is bound to cause some error or uncertainty [61]. Therefore, some dead standing trees of *M. oleifera* could be collected to update our model in further research Figure 9.
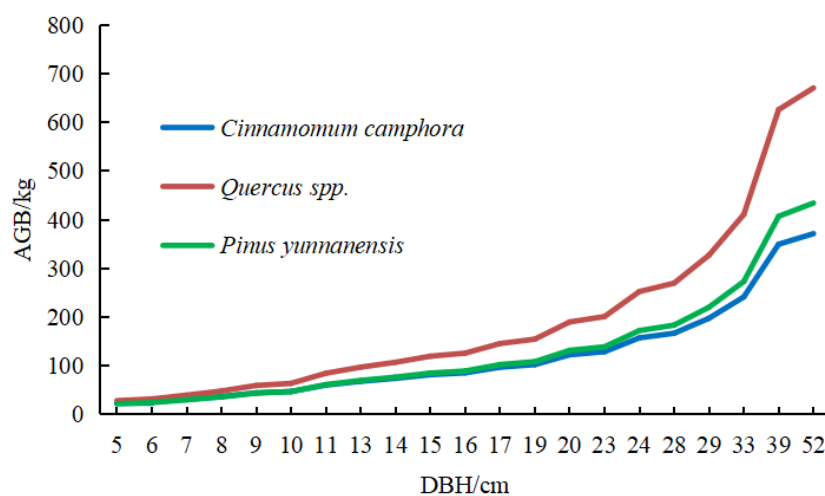

Figure 9. Comparison of multiple tree species' equations for the AGB estimation of *M. oleifera*.

5. Conclusions

The estimation of AGB is crucial for monitoring, managing, developing, and utilizing the resources of *M. oleifera*, a monotypic genus of a national secondary protected plant. In this study, the combination of centimeter-level UAV-RGB remote sensing images (3.5 cm/pixel) and the Mask R-CNN model was employed to accurately identify and extract the canopies of *M. oleifera* in natural mixed forests. The average segmentation accuracy of canopy extraction was 90%. A CA-DBH allometric growth model of individual *M. oleifera* trees (Equation (12)) was established, and the fitting results showed that CA and DBH are highly correlated (R^2 = 0.755). This indicates that CA can be used to estimate the DBH. However, due to the unavailability of experimental materials for the *M. oleifera* tree, an AGB estimation of the individual tree of *M. oleifera* was first attempted using the empirical equation of *Cinnamomum camphora* (Equation (11)). The results of 24 samples showed that

the average AGB was 89.789 kg, the average value of the measured AGB was 84.864 kg, the bias was 6.94 kg, and R^2 was 0.69; in addition, the values of MAE, RMSE, and rRMSE were 23.04 kg, 34.03 kg, and 3.56 kg, respectively. In the future, the Mask R-CNN model will be optimized to achieve high efficiency and accuracy in the extraction of *M. oleifera* tree canopies from centimeter-level resolution UAV-RGB images. Additionally, a three-scale model of *M. oleifera* will be established to extract AGB to provide references for monitoring, managing, developing, and utilizing *M. oleifera* resources.

References

1. Yang, Y.; He, S.L. The complete chloroplast genome of *Malania oleifera* (Olacaceae), an endangered species in China. *Mitochondrial DNA Part B Resour.* **2019**, *4*, 1867–1868. [CrossRef]
2. Yang, T.Q.; Yu, Q.; Xu, W.; Li, D.Z.; Chen, F.; Liu, A.Z. Transcriptome analysis reveals crucial genes involved in the biosynthesis of nervonic acid in woody *Malania oleifera* oilseeds. *Bmc Plant Biol.* **2018**, *18*, 247. [CrossRef] [PubMed]
3. Li, Z.W.; Ma, S.J.; Song, H.; Yang, Z.; Zhao, C.Z.; Taylor, D.; Zhang, M.; Cooke, J. A 3-ketoacyl-CoA synthase 11 (KCS11) homolog from *Malania oleifera* synthesizes nervonic acid in plants rich in 11Z-eicosenoic acid. *Tree Physiol.* **2021**, *41*, 331–342. [CrossRef] [PubMed]
4. Xu, C.Q.; Liu, H.; Zhou, S.S.; Zhang, D.X.; Zhao, W.; Wang, S.; Chen, F.; Sun, Y.Q.; Nie, S.; Jia, K.H.; et al. Genome sequence of *Malania oleifera*, a tree with great value for nervonic acid production. *Gigascience* **2019**, *8*, giy164. [CrossRef]
5. Luo, H.; Xu, J.; Jiao, S.Q.; Zhang, R.G.; Mao, J.F. The complete mitochondrial genome of an endangered tree: *Malania oleifera*. *Mitochondrial DNA Part B Resour.* **2020**, *5*, 3829–3830. [CrossRef] [PubMed]
6. Tu, X.H.; Wan, J.Y.; Xie, Y.; Wei, F.; Quek, S.; Lv, X.; Du, L.Q.; Chen, H. Lipid analysis of three special nervonic acid resources in China. *Oil Crop Sci.* **2020**, *5*, 180–186. [CrossRef]
7. Wang, S.H.; Chen, J.; Yang, W.; Hua, M.; Ma, Y.P. Fruiting character variability in wild individuals of *Malania oleifera*, a highly valued endemic species. *Sci. Rep.* **2021**, *11*, 23605. [CrossRef]
8. Li, B.; Xu, X.M.; Zhang, L.; Han, J.W.; Bian, C.S.; Li, G.C.; Liu, J.G.; Jin, L.P. Above-ground biomass estimation and yield prediction in potato by using UAV-based RGB and hyperspectral imaging. *Isprs. J. Photogramm.* **2020**, *162*, 161–172. [CrossRef]
9. Wang, F.; Yang, M.; Ma, L.; Zhang, T.; Qin, W.; Li, W.; Zhang, Y.; Sun, Z.; Wang, Z.; Li, F.; et al. Estimation of Above-Ground Biomass of Winter Wheat Based on Consumer-Grade Multi-Spectral UAV. *Remote Sens.* **2022**, *14*, 1251. [CrossRef]
10. Campbell, M.J.; Dennison, P.E.; Kerr, K.L.; Brewer, S.C.; Anderegg, W.R.L. Scaled biomass estimation in woodland ecosystems: Testing the individual and combined capacities of satellite multispectral and lidar data. *Remote Sens. Environ.* **2021**, *262*, 112511. [CrossRef]
11. Jiang, F.G.; Kutia, M.; Ma, K.; Chen, S.; Long, J.P.; Sun, H. Estimating the aboveground biomass of coniferous forest in Northeast China using spectral variables, land surface temperature and soil moisture. *Sci. Total Environ.* **2021**, *785*, 147335. [CrossRef] [PubMed]
12. Siddique, M.R.H.; Mahmood, H.; Siddiqui, M.B.N.; Abdullah, S.M.R.; Akhter, M.; Sola, G.; Iqbal, M.Z.; Henry, M. Conventional and additive models for estimating the biomass, carbon and nutrient stock in individual Shorea robusta Gaertn. f. tree of the Sal forests of Bangladesh. *Environ. Chall.* **2021**, *4*, 100178. [CrossRef]
13. Lemi, T.; Eshete, A.; Seid, G.; Mulugeta, S.; Egeta, D.; Teshome, M. Aboveground Biomass Models for Indigenous Tree Species in the Dry Afromontane Forest, Central Ethiopia. *Int. J. For. Res.* **2023**, *2023*, 4901521. [CrossRef]
14. Wang, G.S.; Wang, N.; Guo, W.L. Modelling Forest Aboveground Biomass Based on GF-3 Dual-Polarized and WorldView-3 Data: A Case Study in Datong National Wetland Park, China. *Math. Probl. Eng.* **2021**, *2021*, 9925940. [CrossRef]
15. Kou, W.L.; Dong, J.W.; Xiao, X.M.; Hernandez, A.J.; Qin, Y.W.; Zhang, G.L.; Chen, B.Q.; Lu, N.; Doughty, R. Expansion dynamics of deciduous rubber plantations in Xishuangbanna, China during 2000-2010. *GIScience Remote Sens.* **2018**, *55*, 905–925. [CrossRef]

16. Gesta, J.L.E.; Fernandez, J.M.; Lina, R.S.; Santillan, J.R. Aboveground Biomass and Carbon Stock Estimation of Falcata Through the Synergistic Use of Sentinel-1 and Sentinel-2 Images. *Int. Arch. Photogramm. Remote Sens. Spat. Inf. Sci.* **2023**, *48*, 117–122. [CrossRef]

17. Feng, X.L.; Tang, L.; Xu, M.H. Estimating the biomass of rice by combining GF-1 and RADARSAT-2 data. *Arab. J. Geosci.* **2021**, *14*, 2124. [CrossRef]

18. Han, D.; Yang, H.; Qiu, C.; Yang, G.; Chen, E.; Du, Y.; Yang, W.; Zhou, C. Estimating wheat biomass from GF-3 data and a polarized water cloud model. *Remote Sens. Lett.* **2019**, *10*, 234–243. [CrossRef]

19. Akhtar, A.M.; Qazi, W.A.; Ahmad, S.R.; Gilani, H.; Mahmood, S.A.; Rasool, A. Integration of high-resolution optical and SAR satellite remote sensing datasets for aboveground biomass estimation in subtropical pine forest, Pakistan. *Environ. Monit. Assess.* **2020**, *192*, 584. [CrossRef]

20. Li, H.T.; Kato, T.; Hayashi, M.; Wu, L. Estimation of Forest Aboveground Biomass of Two Major Conifers in Ibaraki Prefecture, Japan, from PALSAR-2 and Sentinel-2 Data. *Remote Sens.* **2022**, *14*, 468. [CrossRef]

21. Quang, N.H.; Quinn, C.H.; Carrie, R.; Stringer, L.C.; Hue, L.T.V.; Hackney, C.R.; Tan, D.V. Comparisons of regression and machine learning methods for estimating mangrove above-ground biomass using multiple remote sensing data in the red River Estuaries of Vietnam. *Remote Sens. Appl.* **2022**, *26*, 100725. [CrossRef]

22. Ramachandran, N.; Saatchi, S.; Tebaldini, S.; Alessandro, M.M.; Dikshit, O. Mapping tropical forest aboveground biomass using airborne SAR tomography. *Sci. Rep.* **2023**, *13*, 6233. [CrossRef] [PubMed]

23. Jos, G.; Mansor, S.; Matthew, N.K. A Review: Forest Aboveground Biomass (AGB) Estimation Using Satellite Remote Sensing. *J. Remote Sens. GIS* **2021**, *10*, 241.

24. Liang, Y.Y.; Kou, W.L.; Lai, H.Y.; Wang, J.; Wang, Q.H.; Xu, W.H.; Wang, H.; Lu, N. Improved estimation of aboveground biomass in rubber plantations by fusing spectral and textural information from UAV-based RGB imagery. *Ecol. Indic.* **2022**, *142*, 109286. [CrossRef]

25. Kou, W.L.; Xiao, X.M.; Dong, J.W.; Gan, S.; Zhai, D.L.; Zhang, G.L.; Qin, Y.W.; Li, L. Mapping Deciduous Rubber Plantation Areas and Stand Ages with PALSAR and Landsat Images. *Remote Sens.* **2015**, *7*, 1048–1073. [CrossRef]

26. Ehlers, D.; Wang, C.; Coulston, J.; Zhang, Y.; Pavelsky, T.; Frankenberg, E.; Woodcock, C.; Song, C. Mapping Forest Aboveground Biomass Using Multisource Remotely Sensed Data. *Remote Sens.* **2022**, *14*, 1115. [CrossRef]

27. Tian, Y.C.; Zhang, Q.; Huang, H.; Huang, Y.J.; Tao, J.; Zhou, G.Q.; Zhang, Y.L.; Yang, Y.W.; Lin, J.L. Aboveground biomass of typical invasive mangroves and its distribution patterns using UAV-LiDAR data in a subtropical estuary: Maoling River estuary, Guangxi, China. *Ecol. Indic.* **2022**, *136*, 108694. [CrossRef]

28. Wei, Q.P.; Yu, G.B.; Jian, M.D.; Hong, Y.Y.; Xi, P.Z.; Yong, C.K. Classification of Grassland Desertification in China Based on vis-NIR UAV Hyperspectral Remote Sensing. *Spectroscopy* **2020**, *35*, 31.

29. Mao, P.; Qin, L.; Hao, M.; Zhao, W.; Luo, J.; Qiu, X.; Xu, L.; Xiong, Y.; Ran, Y.; Yan, C.; et al. An improved approach to estimate above-ground volume and biomass of desert shrub communities based on UAV RGB images. *Ecol. Indic.* **2021**, *125*, 107494. [CrossRef]

30. Tian, Y.C.; Huang, H.; Zhou, G.Q.; Zhang, Q.; Tao, J.; Zhang, Y.L.; Lin, J.L. Aboveground mangrove biomass estimation in Beibu Gulf using machine learning and UAV remote sensing. *Sci. Total Environ.* **2021**, *781*, 146816. [CrossRef]

31. Abdullah, M.M.; Al-Ali, Z.M.; Srinivasan, S. The use of UAV-based remote sensing to estimate biomass and carbon stock for native desert shrubs. *MethodsX.* **2021**, *8*, 101399. [CrossRef] [PubMed]

32. Qin, S.Z.; Nie, S.; Guan, Y.S.; Zhang, D.; Wang, C.; Zhang, X.L. Forest emissions reduction assessment using airborne LiDAR for biomass estimation. *Resour. Conserv. Recycl.* **2022**, *181*, 106224. [CrossRef]

33. Zhang, H.F.; Tang, Z.G.; Wang, B.Y.; Meng, B.P.; Qin, Y.; Sun, Y.; Lv, Y.Y.; Zhang, J.G.; Yi, S.H. A non-destructive method for rapid acquisition of grassland aboveground biomass for satellite ground verification using UAV RGB images. *Glob. Ecol. Conserv.* **2022**, *33*, e1999. [CrossRef]

34. Kashongwe, H.B.; Roy, D.P.; Skole, D.L. Examination of the amount of GEDI data required to characterize central Africa tropical forest aboveground biomass at REDD+ project scale in Mai Ndombe province. *Sci. Remote Sens.* **2023**, *7*, 100091. [CrossRef]

35. Torre-Tojal, L.; Bastarrika, A.; Boyano, A.; Lopez-Guede, J.M.; Graña, M. Above-ground biomass estimation from LiDAR data using random forest algorithms. *J. Comput. Sci.* **2022**, *58*, 101517. [CrossRef]

36. Shu, M.Y.; Shen, M.Y.; Dong, Q.Z.; Yang, X.H.; Li, B.G.; Ma, Y.T. Estimating the maize above-ground biomass by constructing the tridimensional concept model based on UAV-based digital and multi-spectral images. *Field Crop. Res.* **2022**, *282*, 108491.

37. Li, W.; Niu, Z.; Chen, H.; Li, D.; Wu, M.; Zhao, W. Remote estimation of canopy height and aboveground biomass of maize using high-resolution stereo images from a low-cost unmanned aerial vehicle system. *Ecol. Indic.* **2016**, *67*, 637–648. [CrossRef]

38. Tang, Y.Q.; Feng, H.; Chen, J.Y.; Chen, Y. ForestResNet: A Deep Learning Algorithm for Forest Image Classification. *J. Phys. Conf. Ser.* **2021**, *2024*, 12053. [CrossRef]

39. Weinstein, B.G.; Marconi, S.; Bohlman, S.; Zare, A.; White, E. Individual Tree-Crown Detection in RGB Imagery Using Semi-Supervised Deep Learning Neural Networks. *Remote Sens.* **2019**, *11*, 1309. [CrossRef]

40. Xi, Y.B.; Ren, C.Y.; Wang, Z.M.; Wei, S.Q.; Bai, J.L.; Zhang, B.; Xiang, H.X.; Chen, L. Mapping Tree Species Composition Using OHS-1 Hyperspectral Data and Deep Learning Algorithms in Changbai Mountains, Northeast China. *Forests* **2019**, *10*, 818. [CrossRef]

41. Yao, L.; Liu, T.; Qin, J.; Lu, N.; Zhou, C. Tree counting with high spatial-resolution satellite imagery based on deep neural networks. *Ecol. Indic.* **2021**, *125*, 107591. [CrossRef]
42. Schiefer, F.; Kattenborn, T.; Frick, A.; Frey, J.; Schall, P.; Koch, B.; Schmidtlein, S. Mapping forest tree species in high resolution UAV-based RGB-imagery by means of convolutional neural networks. *ISPRS J. Photogramm. Remote Sens.* **2020**, *170*, 205–215. [CrossRef]
43. Ogana, F.N.; Ercanli, I. Modelling height-diameter relationships in complex tropical rain forest ecosystems using deep learning algorithm. *J. For. Res.* **2021**, *33*, 883–898. [CrossRef]
44. Pérez-Carrasco, M.; Karelovic, B.; Molina, R.; Saavedra, R.; Cerulo, P.; Cabrera-Vives, G. Precision silviculture: Use of UAVs and comparison of deep learning models for the identification and segmentation of tree crowns in pine crops. *Int. J. Digit. Earth* **2022**, *15*, 2223–2238. [CrossRef]
45. Castro, W.; Marcato, J.J.; Polidoro, C.; Osco, L.P.; Goncalves, W.; Rodrigues, L.; Santos, M.; Jank, L.; Barrios, S.; Valle, C.; et al. Deep Learning Applied to Phenotyping of Biomass in Forages with UAV-Based RGB Imagery. *Sensors* **2020**, *20*, 4802. [CrossRef]
46. Zhu, Y.F.; Li, D.N.; Fan, J.C.; Zhang, H.Q.; Eichhorn, M.P.; Wang, X.J.; Yun, T. A reinterpretation of the gap fraction of tree crowns from the perspectives of computer graphics and porous media theory. *Front. Plant Sci.* **2023**, *14*, 1109443. [CrossRef]
47. He, K.M.; Gkioxari, G.; Dollar, P.; Girshick, R. Mask R-CNN. *IEEE Trans. Pattern Anal. Mach. Intell.* **2020**, *42*, 386–397. [CrossRef]
48. Gogineni, A.K.; Kishore, R.; Raj, P.; Naik, S.; Sahu, K.K. *Unsupervised Clustering Algorithm as Region of Interest Proposals for Cancer Detection Using CNN*; Springer International Publishing: Cham, Switzerland, 2020; pp. 1386–1396.
49. Lu, N.; Wu, Y.P.; Zheng, H.B.; Yao, X.; Zhu, Y.; Cao, W.X.; Cheng, T. An assessment of multi-view spectral information from UAV-based color-infrared images for improved estimation of nitrogen nutrition status in winter wheat. *Precis. Agric.* **2022**, *23*, 1653–1674. [CrossRef]
50. Lyons, M.B.; Keith, D.A.; Phinn, S.R.; Mason, T.J.; Elith, J. A comparison of resampling methods for remote sensing classification and accuracy assessment. *Remote Sens. Environ.* **2018**, *208*, 145–153. [CrossRef]
51. Li, S.G. Malania, a new genus of oil-yielding plant. *Bull. Bot. Iab. North-East. Forest. Inst.* **1980**, *6*, 67–72.
52. Meng, C. Study on the Aboveground Biomass Model of *Cinamomum camphora* in Urban. Master's Thesis, Beijing Forestry University, Beijing, China, 2011.
53. Wei, C.; Li, H.L.; Cui, G.Q.; Ma, C.H.; Deng, R.G.; Zou, Z.R.; Liu, Z.Z. Efficient separation of *Cinnamomum camphora* leaf essential oil and in vitro evaluation of its antifungal activity. *Arab. J. Chem.* **2022**, *15*, 104225. [CrossRef]
54. Zhang, C.; Liu, H.H.; Huang, N.; Zhang, F.Y.; Meng, Y.Q.; Wang, J.A.; Li, Y.Y. Coordination of leaf hydraulic and economic traits in *Cinnamomum camphora* under impervious pavement. *BMC Plant Biol.* **2022**, *22*, 347. [CrossRef] [PubMed]
55. Yang, C.H.; Wang, Z.; Xiong, L.y.; Liu, Y.P.; Kang, X.L.; Zhao, W.H. Identification and Reconstruction of Citrus Branches under Complex Background Based on Mask R-CNN. *Trans. Chin. Soc. Agric. Mach.* **2019**, *50*, 22–30.
56. He, Y.Y.; Zhang, Y.B.; Li, J.Q. Estimation of stem biomass of individual Abies faxoniana through unmanned aerial vehicle remote sensing. *J. Beijing For. Univ.* **2016**, *38*, 42–49.
57. Liu, Y.D. Study on Biological Characteristics of Young *Aquilaria sinensis* Forest in Southern Fujian. *For. Prospect. Des.* **2015**, *2*, 77–81.
58. Tang, J.W.; Pang, J.P.; Chen, M.Y.; Guo, X.M.; Zeng, R. Biomass and its estimation model of rubber plantations in Xishuangbanna, Southwest China. *Chin. J. Ecol.* **2009**, *28*, 1942–1948.
59. *LY/T 2262-2014*; Tree Biomass Models and Related Parameters to Carbon Accounting for Pinus yunnanensis. China Standard Press: Beijing, China, 2015.
60. *LY/T 2658-2016*; Tree Biomass Models and Related Parameters to Carbon Accounting for Quercus. China Standard Press: Beijing, China, 2017.
61. Aneseyee, A.B.; Soromessa, T.; Elias, E.; Feyisa, G.L. Allometric equations for selected *Acacia* species (*Vachellia* and *Senegalia* genera) of Ethiopia. *Carbon Balance Manag.* **2021**, *16*, 34. [CrossRef]